

ISTITUTO NAZIONALE DI FISICA NUCLEARE

Laboratori Nazionali  
di Legnaro

INFN/BE-81/10  
18 Giugno 1981

P. Boccaccio and L. Vannucci: CURRENT PULSE PICKOFF  
TECHNIQUE WITH SURFACE-BARRIER DETECTORS.

Istituto Nazionale di Fisica Nucleare  
Laboratori Nazionali di Legnaro

INFN/BE-81/10  
18 giugno 1981

P. Boccaccio and L. Vannucci:

## CURRENT PULSE PICKOFF TECHNIQUE WITH SURFACE-BARRIER DETECTORS

### ABSTRACT.

Preliminary results of an experimental investigation on the current pulse pickoff technique with surface-barrier detectors are presented. Detector pulse amplitude and rise-time calculations, employing a recent model for plasma effects, show a fairly good agreement with experimental waveforms. Possible applications of the technique to heavy-ion timing experiments are discussed.

### 1. - INTRODUCTION.

In recent years considerable progress was achieved in developing experimental techniques for the identification of nuclear reaction products from heavy-ion collisions.

Mass identification techniques based on particle time-of-flight (TOF) and energy measurements are widely employed in ion detection systems. By independent measurements of ion velocity and energy, mass can be determined and the experimental mass resolving power ( $\Delta A/A$ ) can be estimated from the relative energy ( $\Delta E/E$ ) and time ( $\Delta t/t$ ) resolution<sup>(1)</sup>:

$$\frac{\Delta A}{A} = \left[ \left( \frac{\Delta E}{E} \right)^2 + \left( 2 \frac{\Delta t}{t} \right)^2 \right]^{1/2} \quad (1)$$

Surface-barrier detectors (SBD) are widely employed as stop detectors in TOF spectrometers, because of their excellent energy resolution and fast response. Recent measurements of SBD energy resolution for heavy ions can be approximately reproduced by the formula<sup>(2)</sup>:

$$\frac{\Delta E}{E} \approx 5 \times 10^{-3} \left( \frac{E}{A} \right)^{-1/2} (1 + 0.01 A) \quad (2)$$

in which the ion energy ( $E$ ) is in MeV and the mass ( $A$ ) in amu. Time resolutions of the order of 100 ps were reported<sup>(3-5)</sup> for  $\Delta E$ - $E$  TOF telescopes employing surface-barrier detectors, which allowed ion mass identification up to 20 amu. A mass resolving power  $\Delta A/A = 1/70$  was obtained with a secondary-electron start detector and a SBD stop detector<sup>(6)</sup>, allowing the separation of the isotopes  $^{79}\text{Br}$  and  $^{81}\text{Br}$  ( $E/A = 1$  MeV/amu). Ion identification in the range  $60 \leq A \leq 208$  was achieved for ion energies from 300 to 1200 MeV<sup>(7)</sup>, with silicon detector  $\Delta E$ - $E$  TOF telescopes.

Analysis of formulas (1), (2), indicates that limitations to mass resolving power are imposed mainly by energy resolution for heavy ( $A \gtrsim 100$ ) ions, while for lighter ions time resolution is more important. The relative time resolution ( $\Delta t/t$ ) can be made, in principle, arbitrarily small with a suitable choice of the flight path length; however, for practical reasons and to avoid excessively small solid angles, restrictions have to be made on the lengths of the flight paths.

A further reduction of the relative time resolution can be achieved, for a given flight path length, by minimizing the overall time resolution ( $\Delta t$ ); in this way complete mass resolution can be extended to wider regions of the ( $\frac{E}{A}, A$ ) plane<sup>(2)</sup>.

The study of SBD timing characteristics indicates that excellent time resolutions can be obtained, provided that suitable signal pickoff and processing techniques are employed<sup>(8)</sup>. Constant-fraction discriminators (CFD) are conveniently employed in timing applications with surface-barrier detectors to minimize the timing uncertainty caused by time walk and jitter. As noise-induced time jitter is inversely proportional to the CFD input signal slope, fast signals are particularly suitable for high timing accuracy<sup>(9)</sup>. Moreover, also the time walk due to the charge sensitivity of the CFD Zero-crossing detector is minimized.

In this respect, fast pickoff techniques are being continuously studied and improved in performances because of their importance in time spectrometry. SBD time signals are usually obtained by differentiating pulses from a charge sensitive amplifier, or shunting the charge amplifier with a fast voltage amplifier.

Alternatively, SBD signals can be applied to the input of a fast low-impedance amplifier, in which case true current pulses are employed as timing signals. This technique was studied by some authors<sup>(8, 10)</sup> and employed in few light-ion timing experiments<sup>(11, 12)</sup>; applications are found in recent studies on "plasma time" effects in surface-barrier detectors<sup>(13-15, 18)</sup>.

In the present paper preliminary results of an experimental investigation on the current pulse pickoff technique are reported, employing both light and heavy ions from radioactive sources. Possible applications to heavy-ion timing experiments are discussed and some comparisons are made with the voltage pulse pickoff technique.

## 2. - VOLTAGE AND CURRENT PULSE PICKOFF TECHNIQUES.

Energy and time signals associated with the detection of a charged particle inside a SBD can be obtained with the use of different techniques<sup>(8)</sup>. Generally, care must be taken to minimize interactions between the energy and time channels, as well as noise injection, which dete

riorates the energy and time resolution.

In the arrangement of Fig. 1a time signals supplied by a SBD are applied to a fast amplifier with a high and mainly capacitive input impedance<sup>(16)</sup> (voltage amplifier). The charge amplifier is usually connected to the SBD through a resistor (R) or a resistor-inductor (R-L) parallel connection. Voltage pulse rise times at the fast amplifier input are mainly determined by the SBD charge collection time and the time constant of the detector equivalent circuit, loaded by the amplifier input capacitance.

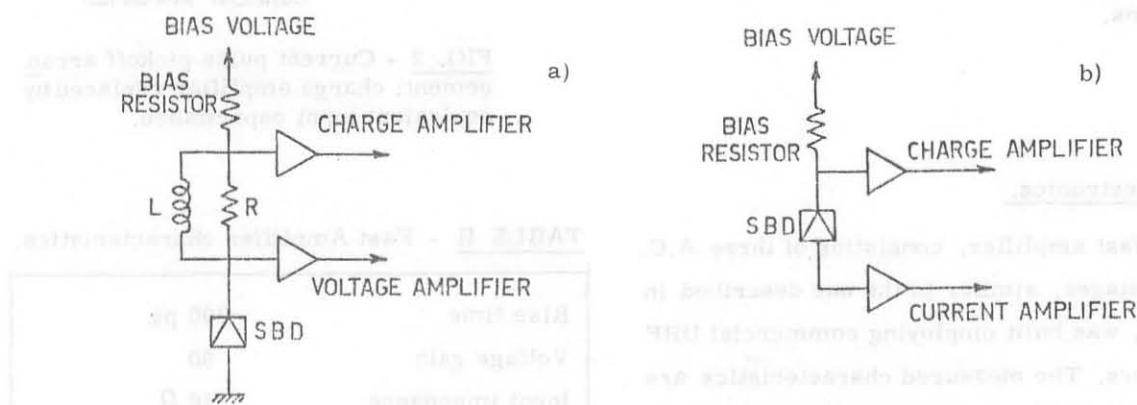


FIG. 1 - Fast signal pickoff arrangements.

In the complementary arrangement of Fig. 1b the SBD current pulses are applied to the input stage of a fast amplifier with low and mainly resistive impedance. Current pulse rise times are mainly determined by the time constant of the detector equivalent circuit, loaded by the amplifier input resistance, if other effects (e.g. the "plasma time", which will be discussed later), are negligible. In this case, separation between the energy and time channel is provided by the detector equivalent resistive-capacitive network, according to the equivalent circuit of Sect. 4.1. An advantage of this technique consists in the use of a low-impedance terminated cable to connect the SBD to the time channel electronics, with considerable reduction of additional capacitance.

### 3. - EXPERIMENTAL.

Using the arrangement of Fig. 1b, current pulses were observed from three silicon surface-barrier detectors excited by  $^{244}\text{Cm}$   $\alpha$ -particles and  $^{252}\text{Cf}$  fission fragments. Detector specifications are given in Table I. A Canberra mod. 2003BT charge amplifier was employed, and the fast amplifier described in Sect. 3.1.

TABLE I - Detector specifications.

Detector	$\rho(\Omega \cdot \text{cm})$	Slice thickness ( $\mu\text{m}$ )
D1(x)	1400	100
D2(o)	5000	230
D3(x)	1200	100

(x) A Series Ortec Detector; 50 mm<sup>2</sup> active area.

(o) Manufactured in the Munich University detector laboratory; 200 mm<sup>2</sup> active area.

In several measurements, the charge amplifier was replaced with a R-C network, as shown in Fig. 2. Waveforms obtained with the arrangement of Fig. 1b were compared to those ones obtained with the arrangement of Fig. 2, to study the influence of the time-dependent charge amplifier input impedance<sup>(17)</sup>.

A Tektronik mod. 485 oscilloscope was employed to display detector pulses and a polaroid camera to record waveforms.

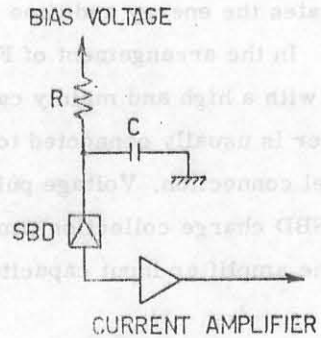


FIG. 2 - Current pulse pickoff arrangement; charge amplifier replaced by equivalent input capacitance.

3.1. - Electronics.

A fast amplifier, consisting of three A.C. coupled stages, similar to the one described in Ref. (19), was built employing commercial UHF transistors. The measured characteristics are reported in Table II and the circuit is drawn in Fig. 3. The output noise level was measured with a Hewlett-Packard (HP) mod. 3400 A r.m.s.

TABLE II - Fast Amplifier characteristics.

Rise time	700 ps
Voltage gain	60
Input impedance	120 $\Omega$
Noise (referred to input)	<45 $\mu$ V r. m. s.

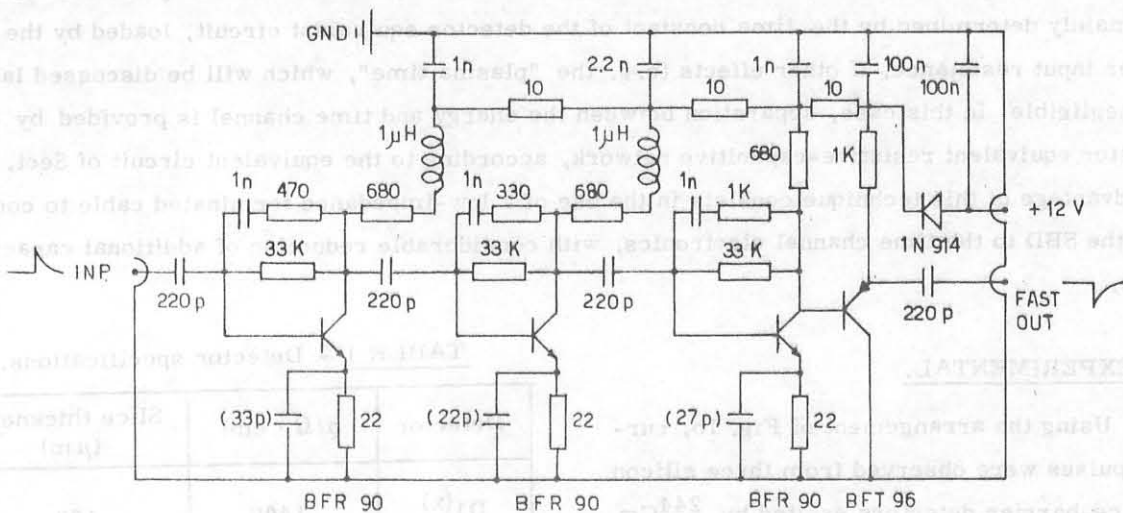


FIG. 3 - Fast amplifier circuit.

voltmeter. The intrinsic rise time was measured with a HP mod. 1105 A tunnel diode pulser (rise-time < 20 ps), a Marconi Instruments mod. TF 2163 UHF attenuator and a HP sampling oscilloscope (mod. 1811 A Vertical amplifier with mod. 1430 C sampler).

### 3.2. - Detector current pulses.

Figs. 4-6 display the recorded waveforms relative to some representative experimental conditions. Figs. 6a,b refer to the arrangement of Fig. 1b; other waveforms were obtained with the arrangement of Fig. 2 with  $R = 18 \text{ M}\Omega$ ,  $C = 110 \text{ pF}$ .

Fig. 6b displays detector D3 waveforms, relative to  $^{244}\text{Cm}$   $\alpha$ -particles, at the current amplifier output. Pulse rise time, accounting for the amplifier (0.7 ns) and oscilloscope (1 ns) rise times, is about 1 ns with  $\approx 16 \mu\text{A}$  peak amplitude for an electric field of  $2.5 \times 10^6 \text{ V/m}$ .

Fission fragment induced pulses are displayed in Figs. 4a, 5a, as seen at the current amplifier input; the corresponding amplified pulses are displayed in Figs. 4b, 5b. In this case, pulse rise times and peak amplitudes are respectively 4 ns, 600  $\mu\text{A}$  (Fig. 4a) and 8 ns, 240  $\mu\text{A}$  (Fig. 5a), depending on the different detectors (D1, D2, respectively) and electric fields ( $2.5 \times 10^6 \text{ V/m}$ ,  $1.1 \times 10^6 \text{ V/m}$ , respectively) employed.

Common features exhibited by such waveforms consist in nearly symmetrical rise and fall edges, with essentially no flat top, and a time width of few nanoseconds.

Flat-top waveforms reported in Ref. (15) are related to different experimental conditions (e. g. detector thickness, field intensity), as will be discussed later.

Fig. 6a displays waveforms obtained in the same conditions as for Fig. 4a, except for the insertion of the charge amplifier. Variations in pulse amplitude and rise time are reasonably well explained considering the different time constants associated with the charge amplifier equivalent circuit and the R-C network. In no case, however, pulse shape distortions due to the time variation of the charge amplifier input impedance were so evident as described in Ref. (17).

Noise-induced degradation in energy resolution was measured with the arrangements of Figs. 1a, 1b, employing  $^{244}\text{Cm}$   $\alpha$ -particles. Inserting the current amplifier the FWHM energy resolution was found to vary from 19.6 to 19.8 keV; with a fast voltage amplifier the measured value was 22 keV. In both arrangements, however, this noise contribution can be small compared to SBD intrinsic energy resolution for heavier ions.

### 4. - CALCULATIONS AND DATA ANALYSIS.

Experimental current pulse shapes were analyzed and compared to calculated waveforms to study the main physical effects which determine signal generation inside a SBD.

Heavy-ion induced pulses were analyzed as a general case, since plasma time effects<sup>(8)</sup> are dominant.

In the calculations the detectors were considered to be strongly overdepleted, such that the internal electric field could be considered constant. Short range particles were assumed to impinge perpendicularly on the p-side of a n-type silicon detector and electron transport only was considered to contribute to charge induction.

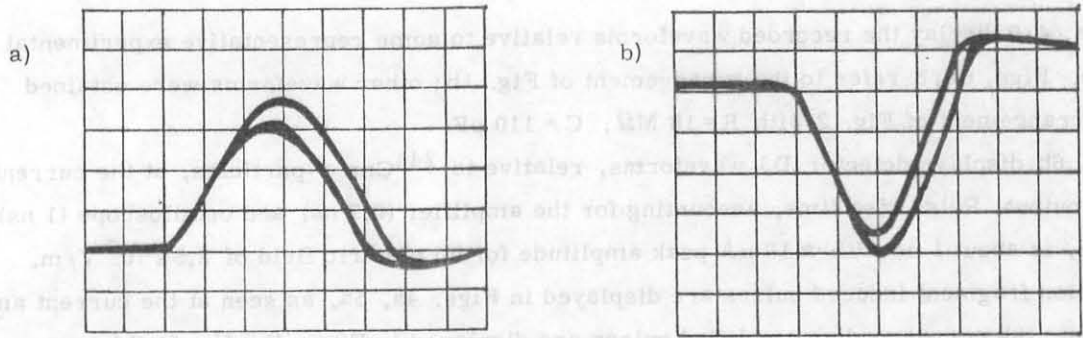


FIG. 4 - Fission fragment current pulses from detector D1,  $V_B = 250$  V. Horizontal sensitivity: 2 ns/main division. a) Fast amplifier input signal; b) Output pulse.

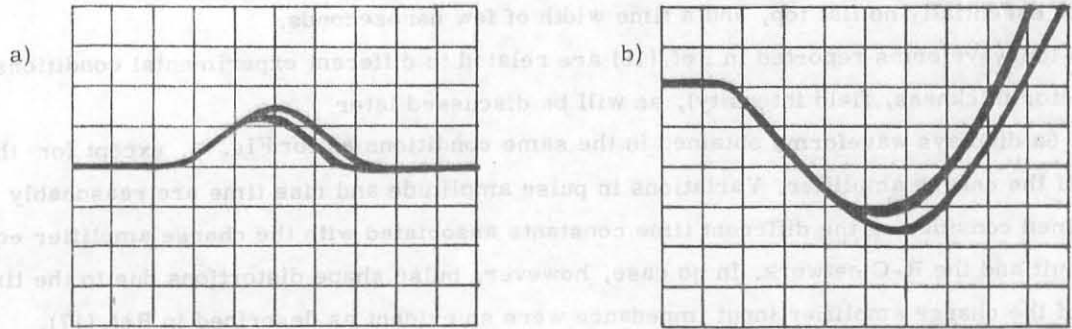


FIG. 5 - Fission fragment current pulses from detector D2,  $V_B = 250$  V. a) Fast amplifier input signal; horizontal sensitivity: 5 ns/main division. b) Output pulse; horizontal sensitivity: 2 ns/main division.

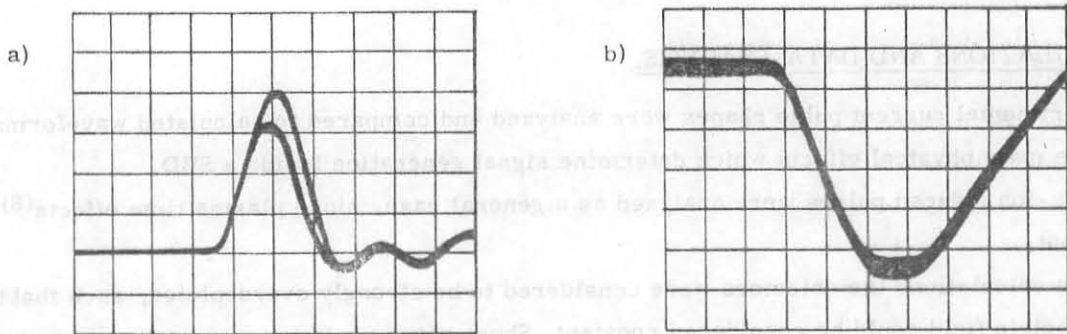


FIG. 6 - a) Current pulse shape recorded as for Fig. 4a, except for the insertion of the charge amplifier; Horizontal sensitivity: 5 ns/main division. b)  $^{244}\text{Cm}$ -particle current pulse from detector D3 at the fast amplifier output,  $V_B = 240$  V; Horizontal sensitivity: 1 ns/main division.

4.1. - Equivalent circuit.

Fig. 7 displays the equivalent circuit relative to the experimental arrangement of Fig. 1b. The simplified detector equivalent circuit consists of a current generator  $i(t)$  connected to the detector capacitance  $C_0$ . The external circuit is represented by  $C_1$  which stands for the charge amplifier input capacitance and stray capacitances, and  $R_1$ , the current amplifier input resistance. This equivalent circuit applies also to the arrangement of Fig. 2 with the correspondence:  $C_1 = C$ .

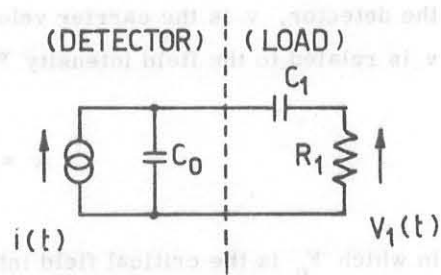


FIG. 7 - Detector and load equivalent circuit.

The time dependence of voltage  $V_1$  at the fast amplifier input can be found solving the differential equation:

$$\frac{dV_1}{dt} + \frac{V_1}{\tau} = \frac{i}{C_0} \tag{3}$$

in which  $i$  is the generator current and  $\tau$  the equivalent circuit time constant:

$$\tau = R_1 \left( \frac{1}{C_0} + \frac{1}{C_1} \right)^{-1} \tag{4}$$

4.2. - Charge induction process.

As the time for an incident ion to stop inside the detector is very small compared to the electron drift time<sup>(20)</sup>, it is assumed that at  $t=0$  an ionization track is created and the first charge carriers start moving under the electric field influence. However, not all the charge carrier start moving immediately, since a finite time  $t_p$  is needed for the field to penetrate into the plasma column generated by the incident particle. According to the theoretical model described in Ref. (14), the rate of charge release  $dq^+/dt$  from the plasma region is:

$$\frac{dq^+}{dt} = 3Q_0 \frac{t^2}{t_p^3} \tag{5}$$

in which  $Q_0$  is the total ionization charge created by the incident particle,  $t_p$  the plasma time:

$$t_p = 1.32 \times 10^{-10} \frac{(n_1 E)^{1/3}}{F} \tag{6}$$


which depends on the electric field  $F$ , the ion energy  $E$  and the initial linear ionization density in the track  $n_1$ .

At any time  $t$ , the current  $i$  induced by charge carrier motion through the detector is given by:

$$i(t) = q(t) \frac{v}{w} \tag{7}$$



according to the generalized Ramo's theorem<sup>(21)</sup>;  $q(t)$  stands for the total charge moving through the detector,  $v$  is the carrier velocity and  $w$  the detector thickness. The electron drift velocity  $v$  is related to the field intensity  $F$  through the relationship:



$$v = \begin{cases} \mu_0 F & , F \leq F_c \\ \mu_0 (F_c F)^{1/2} & , F > F_c \end{cases} \quad (8)$$

in which  $F_c$  is the critical field intensity for electrons and  $\mu_0$  the electron low-field mobility<sup>(22)</sup>.

For a bias voltage  $V_B$  much larger than the total depletion voltage  $V_t$ , the electric field can be considered constant, i. e. :

$$F = \frac{V_B}{w} \quad (9)$$

as well as the electron drift velocity, for constant temperature. This assumption becomes exact when high fields are employed such that the saturation limit for electron velocity in silicon is reached ( $v_{\max} \sim 10^5$  m/s).

The usual expression for SBD current pulses<sup>(23)</sup>:

$$i(t) = \frac{Q_0}{\tau} e^{-t/\tau} \quad (10)$$

is not adequate to the present case, as the underlying hypothesis of a linearly varying field that vanishes at the back contact does not apply. Moreover, no time delay for full charge release is accounted for.

Calculations employing expression (10) yield pulse amplitudes and rise times which are independent on the electric field intensity, in conflict with experimental results reported in Sect. 4.4.

#### 4.3. - Detector pulse shape.

Assuming that the time for the first charge carriers to be collected is:

$$t_1 = \frac{w - R}{v} \quad , \quad (11)$$

in which  $R$  is the ionization track length, two different situations can occur, according to the relative magnitude of  $t_1$  and  $t_p$ :

- a)  $t_p < t_1$ , in which case all charge carriers are drifting in the time interval  $(t_p, t_1)$ , yielding a nearly flat-top current pulse (Fig. 8a);
- b)  $t_1 < t_p$ , in which case charge collection starts before last carrier release from the plasma region; current pulse shapes (Fig. 8b) exhibit no flat top as far as charge emission and collection rates are different.

Situation a) typically occurs with light ions and high electric fields, while the other one is generally related to the detection of strongly ionizing particles.

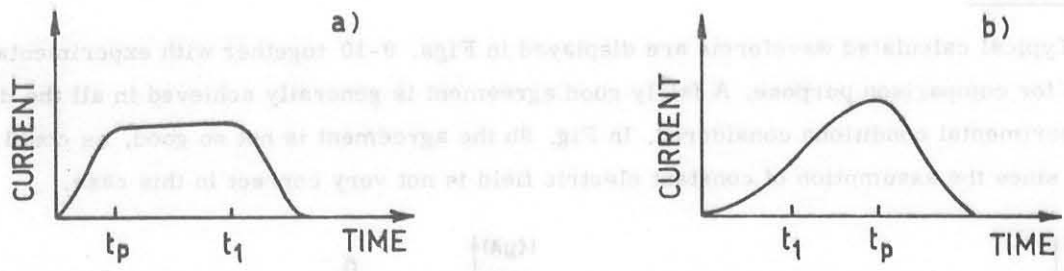


FIG. 8 - Expected current pulse shapes from an overdepleted SBD. a)  $t_p < t_1$ ;  
 b)  $t_1 < t_p$ .

This description can be usefully employed to explain the different pulse shapes in Fig. 3 and 5a of Ref. (15) as will be shown in Sect. 4.4. Moreover, presently calculated values of  $t_1$ ,  $t_p$ , for the conditions reported therein, very well compare to the experimentally defined  $T_k$ ,  $T_p$  values.

Assuming that for all charge carriers the transit time  $t_t$  is the same (i. e.  $t_t = t_1$ , since  $R \ll w$ ), the following expressions for the induced current are found:

a) 
$$i(t) = \begin{cases} Q_0 \frac{v}{w} \left(\frac{t}{t_p}\right)^3, & 0 \leq t \leq t_p \\ Q_0 \frac{v}{w}, & t_p \leq t \leq t_1 \\ Q_0 \frac{v}{w} \left[1 - \left(\frac{t - t_1}{t_p}\right)^3\right], & t_1 \leq t \leq t_1 + t_p \\ 0, & t \geq t_1 + t_p \end{cases} \quad (12)$$

b) 
$$i(t) = \begin{cases} Q_0 \frac{v}{w} \left(\frac{t}{t_p}\right)^3, & 0 \leq t \leq t_1 \\ Q_0 \frac{v}{w} \left(\frac{t_1}{t_p}\right)^3 \left[1 + 3\left(\frac{t}{t_1}\right)^2 - 3\frac{t}{t_1}\right], & t_1 \leq t \leq t_p \\ Q_0 \frac{v}{w} \left(\frac{t_1}{t_p}\right)^3 \left[\left(1 - \frac{t}{t_1}\right)^3 + \left(\frac{t_p}{t_1}\right)^3\right], & t_p \leq t \leq t_1 + t_p \\ 0, & t \geq t_1 + t_p \end{cases} \quad (13)$$

in which the charge collection rate  $d\bar{q}/dt$  at time  $t$  was assumed to be equal to the emission rate at time  $t - t_t$ .

4.4. - Results.

Typical calculated waveforms are displayed in Figs. 9-10 together with experimental pulse shapes for comparison purpose. A fairly good agreement is generally achieved in all the different experimental conditions considered. In Fig. 9b the agreement is not so good, as could be expected since the assumption of constant electric field is not very correct in this case.

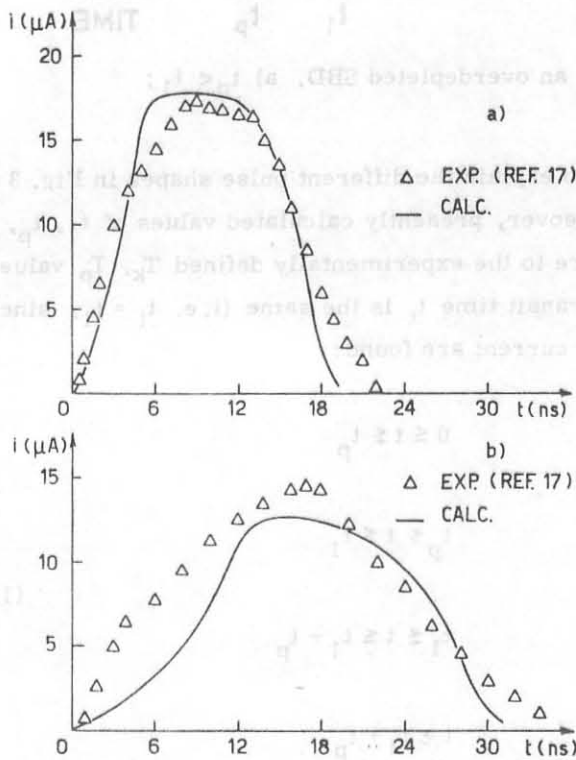


FIG. 9 - Comparison between experimental and calculated waveforms. a) Experimental pulse shape from Fig. 5a of Ref. (15); b) Experimental pulse shape from Fig. 3 of Ref. (15).

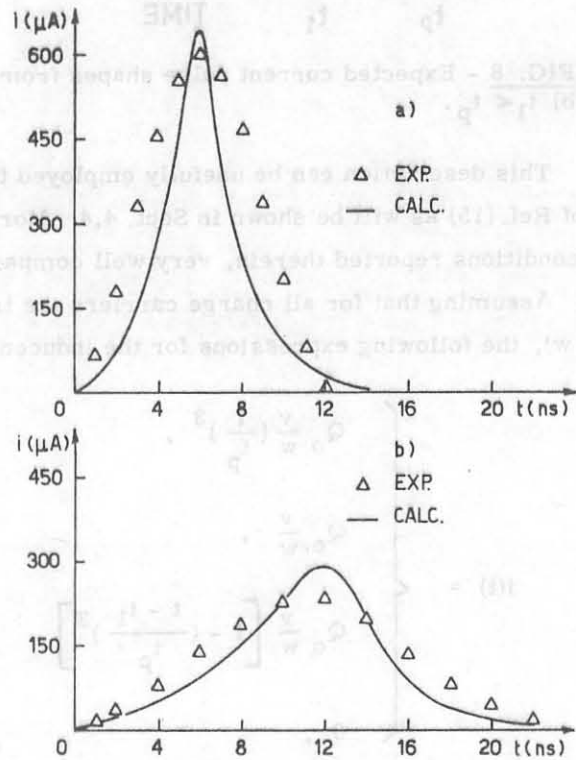


FIG. 10 - Comparison between experimental and calculated waveforms. a) Experimental pulse shape from Fig. 4a; b) Experimental pulse shape from Fig. 5a.

A common characteristic of calculated waveforms consists in a time delay which shifts the beginning of the signal by some nanoseconds. Calculated waveforms in Figs. 9-10 were shifted to the left for easier comparison with experimental shapes; time shifts were 4 ns, 5 ns, respectively, for Figs. 9a, b, and 1 ns, 4ns, respectively, for Figs. 10a, b. The magnitude of such time delays actually depends on the plasma time as a consequence of the expression assumed for the induced current  $i(t)$ .

Although calculated time delays are generally larger than the experimentally measured values<sup>(13, 24-27)</sup>, such qualitative interpretation may be helpful in understanding the plasma delay effect more completely.

Experimental pulse heights and rise times, as a function of electric field intensity, are displayed in Figs. 11a, b, and compared to calculated values, for detectors D1 and D2 excited by

252 Cf fission fragments.

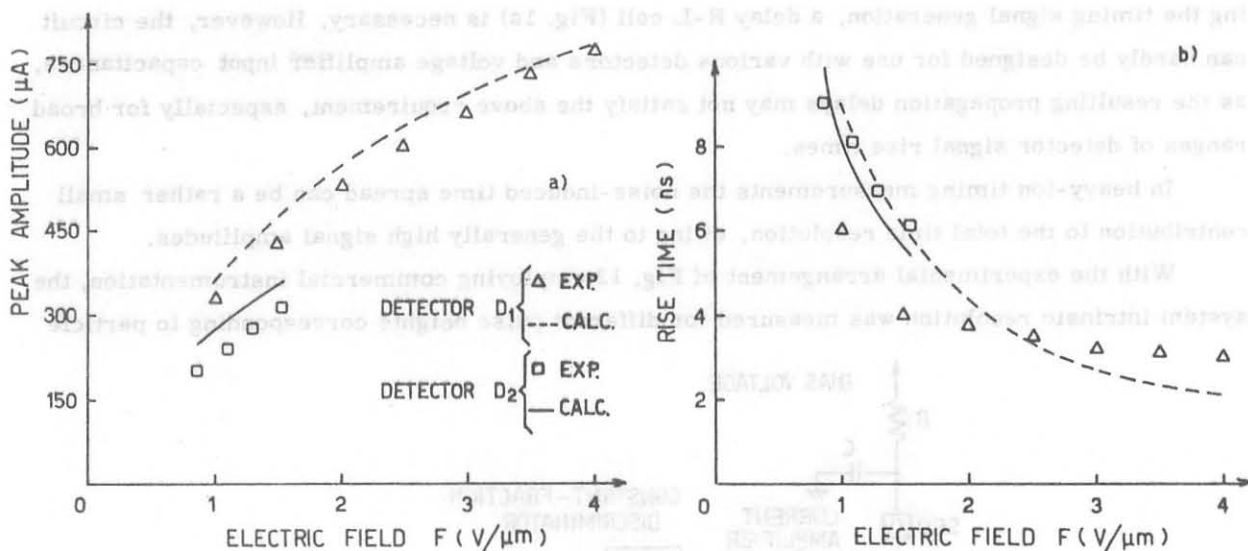


FIG. 11 - Comparison between experimental and calculated data sets. a) Peak pulse amplitude as a function of electric field intensity; b) Pulse rise time as a function of electric field intensity.

Calculated pulse heights are slightly larger than the corresponding experimental values since several effects, as charge trapping and recombination, are not accounted for.

Calculated pulse rise times are closely proportional to the corresponding plasma time, as could be expected; a good agreement with experimental data is generally obtained for high field intensities.

## 5. - DISCUSSION AND CONCLUSIONS.

Current pulses from a SBD can be conveniently employed as timing signals because of their short rise time and width. With the arrangement of Fig. 1b a very short time constant ( $\tau \sim 1$  ns) is normally associated to the equivalent circuit, practically unaffected the signal rise time in most cases.

Current pulse rise time is essentially determined by the plasma time, which depends on the detected ion energy and specific ionization, as well as on the electric field. In this respect, good timing accuracy can be obtained provided that signal amplitude and rise time variations are suitably compensated (e. g. with constant-fraction ARC discriminators<sup>(9)</sup>). Ultimate limitations to timing accuracy are related to plasma time delay jitter<sup>(26)</sup>. The magnitude of this effect was found to be 3% of the total plasma time for <sup>252</sup>Cf fission fragments<sup>(20)</sup>, whereas for  $\alpha$ -particles it was estimated<sup>(24)</sup> to be 10-15%.

With the voltage pulse pickoff technique, in addition to the problems discussed above, the timing signal amplitude may be consistently reduced by plasma time effects. This situation occurs when pulse rise times are comparable to or larger than the time for establishing a virtual

ground in the charge amplifier. To avoid sensible charge transfer to the charge amplifier during the timing signal generation, a delay R-L cell (Fig. 1a) is necessary. However, the circuit can hardly be designed for use with various detectors and voltage amplifier input capacitances, as the resulting propagation delays may not satisfy the above requirement, especially for broad ranges of detector signal rise times.

In heavy-ion timing measurements the noise-induced time spread can be a rather small contribution to the total time resolution, owing to the generally high signal amplitudes.

With the experimental arrangement of Fig. 12 employing commercial instrumentation, the system intrinsic resolution was measured for different pulse heights corresponding to particle

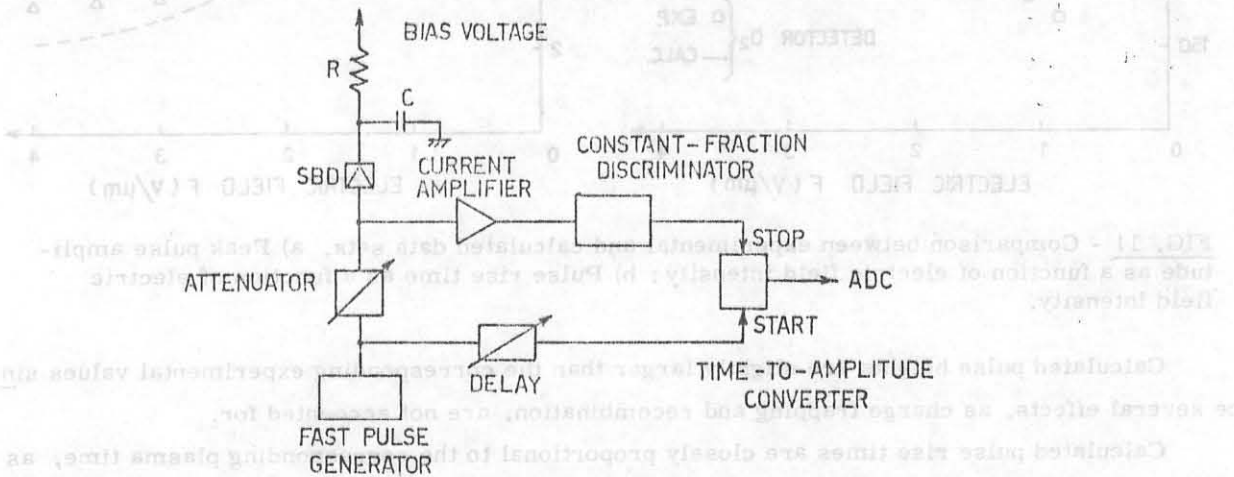


FIG. 12 - Experimental arrangement for intrinsic time resolution measurements.

energies in the range  $E = 6-100$  MeV. Detector D1 was connected to the circuit and a bias voltage  $V_B = 250$  V was applied. The measured FWHM time spread, as a function of pulse height, is shown in Fig. 13. Results are comparable to those ones reported in Refs. (3, 28).

Further precise measurements are needed to investigate plasma time effects in surface-barrier detectors and their influence on timing accuracy. In this respect, heavy ions represent a suitable tool since plasma effects are dominant in the physical processes leading to signal induction. Further developments are correspondingly needed in time pickoff techniques as well as in fast circuitry design.

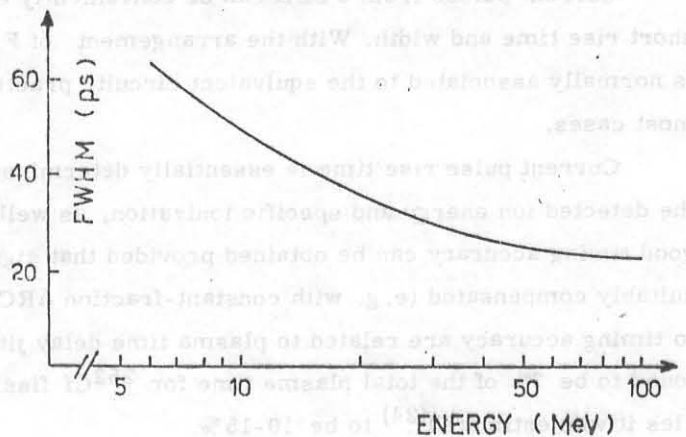


FIG. 13 - Measured FWHM timing spread as a function of pulse height, with the arrangement of Fig. 12.

REFERENCES

- (1) - J. Pouthas, S. Agarwal, M. Engrand and C. Pisani, Nuclear Instr. and Meth. 145, 445 (1977).
- (2) - R. Bass, J. V. Czarnecki and R. Zitzmann, Nuclear Instr. and Meth. 130, 125 (1975).
- (3) - G. W. Butler, A. M. Poskanzer and D. A. Landis, Nuclear Instr. and Meth. 89, 189 (1970).
- (4) - B. Zeidman, W. Henning and D. G. Kovar, Nuclear Instr. and Meth. 118, 361 (1974).
- (5) - H. Pleyer, B. Kohlmeyer, W. F. W. Schneider and R. Bock, Nuclear Instr. and Meth. 96, 263 (1971).
- (6) - W. F. W. Schneider, B. Kohlmeyer, W. Pfeffer, F. Pühlhofer and R. Bock, Nuclear Instr. and Meth. 123, 93 (1975).
- (7) - H. Essel, P. Sperr, K. Hartel, P. Kienle, H. J. Körner, K. E. Rehm and W. Wagner, Nuclear Instr. and Meth. 174, 515 (1980).
- (8) - A. Alberigi Quaranta, M. Martini and G. Ottaviani, IEEE Trans. Nucl. Sci. NS-16, No. 2, 35 (1969).
- (9) - ORTEC Application Note 41.
- (10) - A. Alberigi Quaranta, M. Martini and G. Ottaviani, Nuclear Instr. and Meth. 47, 10 (1967).
- (11) - W. D. Emmerich, A. Hofmann, G. Philipp, K. Thomas, F. Vogler, A. Dittner and J. W. Klein, Nuclear Instr. and Meth. 88, 327 (1970).
- (12) - A. Alberigi Quaranta, A. Taroni and G. Zanarini, Nuclear Instr. and Meth. 72, 72 (1969).
- (13) - L. Hannappel, H. Henschel and R. Schmidt, Nuclear Instr. and Meth. 151, 537 (1978).
- (14) - W. Seibt, K. E. Sundström and P. A. Tove, Nuclear Instr. and Meth. 113, 317 (1973).
- (15) - R. N. Williams and E. M. Lawson, Nuclear Instr. and Meth. 120, 261 (1974).
- (16) - M. Goyot, Nuclear Instr. and Meth. 155, 289 (1978).
- (17) - A. Alberigi Quaranta, M. Martini, G. Ottaviani and G. Zanarini, Nuclear Instr. and Meth. 57, 131 (1967).
- (18) - H. Henschel, H. Hipp, A. Kohnle and F. Gönnerwein, Nuclear Instr. and Meth. 125, 365 (1975).
- (19) - H. Stelzer, Nuclear Instr. and Meth. 133, 409 (1976).
- (20) - P. A. Tove and K. Falk, Nuclear Instr. and Meth. 12, 278 (1961).
- (21) - G. Cavalleri, E. Gatti, G. Fabbri and V. Svelto, Nuclear Instr. and Meth. 92, 137 (1971).
- (22) - P. A. Tove, W. Seibt and W. Leitz, Nuclear Instr. and Meth. 51, 304 (1967).
- (23) - G. Fabbri and V. Svelto, Nuclear Instr. and Meth. 35, 83 (1965).
- (24) - M. Moszynski and B. Bengston, Nuclear Instr. and Meth. 91, 73 (1971).
- (25) - H. O. Neidel and H. Henschel, Nuclear Instr. and Meth. 178, 137 (1980).
- (26) - H. Henschel and R. Schmidt, Nuclear Instr. and Meth. 151, 529 (1978).
- (27) - E. C. Finch, C. F. G. Delaney and M. Asghar, IEEE Trans. Nucl. Sci. NS-27, No. 1, 286 (1980).
- (28) - I. S. Sherman, R. G. Roddick and A. J. Metz, IEEE Trans. Nucl. Sci. NS-15, 500 (1968).